

Long-range nature of surface-enhanced Raman scattering

V. I. Kukushkin,¹ A. B. Van'kov,¹ and I. V. Kukushkin¹

¹*Institute of Solid State Physics, RAS, Chernogolovka 142432, Russia*

(Dated: June 9, 2021)

The long-range action of surface-enhanced Raman scattering (SERS) is probed via distance-dependent measurements of molecular Raman spectra. To this end, identical SERS substrates composed of irregular silver nanoisland arrays were covered by dielectric spacer layers with variable thickness, and the strength of the SERS signal produced from analyte molecules deposited on top of the structure was analyzed. The obtained distance dependence of the signal strength exhibited a shelf-like behavior up to 30 nm away from the enhancing surface and then rapidly decreased further away. Thus, the observed behavior of the electromagnetic mechanism of SERS enhancement in metal island films contradicts the widely accepted picture of extremely rapid (2–3 nm) decay of SERS-enhancement of 2D nanoparticle ensembles. Because of the observed steady enhancement factors at distances of ~ 30 nm from the surface, SERS can be used for probing the spectra of macromolecules or other objects relatively distant from the metal surface.

PACS numbers:

Since its first observation by Fleischmann *et al.* (1974)¹ surface-enhanced Raman scattering (SERS) has been thoroughly investigated as an amazing physical phenomenon itself and one of the most promising tools for analytical applications. The first perception of SERS as a giant enhancement over conventional Raman scattering in experiments of Jeanmaire, Van Duyne² and Albrecht, Creighton³ was followed by an extensive theoretical and experimental analysis, searching for the most general explanation of the enhancement mechanism. The enhancement of Raman scattering signals from organic molecules absorbed on nanostructured metal surfaces and photoexcited in a certain spectral range has been shown to reach 6–10 orders of magnitude^{2,4}. Further enhancement of up to ~ 14 orders of magnitude was observed on molecules residing in silver colloidal aggregates, enabling single molecule detection⁵.

It is now generally agreed that more than one effect contributes to the total enhancement of Raman signals. The enhancement mechanisms are roughly divided into so-called electromagnetic (EM) field enhancement^{6–8} and chemical first-layer effects^{9–11}. The electromagnetic enhancement is caused by the enhanced local optical fields at the place of the molecule nearby the metal surface due to excitation of electromagnetic resonances, called surface plasmon polaritons. For isolated silver or gold spheroidal nanoparticles typical values for electromagnetic enhancement of SERS are on the order of^{12,13} $10^6 - 10^7$.

For the more sophisticated case of closely spaced interacting particles (or clusters of particles), the individual dipole oscillators of the small particles couple, thereby generating normal modes of plasmon excitation that embrace the cluster. According to theoretical evaluations, the excitation is not distributed uniformly over the cluster but tends to be spatially localized in so-called "hot" areas^{14–16}.

Effects of chemical enhancement arise from the electronic coupling between the adsorbate molecule and the

metal surface and excitation of adsorbate-localized electronic resonances (or charge transfer resonances). The chemical enhancement is valid solely for molecules in direct contact with the metal surface, and hence, it is referred to as a first-layer enhancement. The magnitude of chemical enhancement has been estimated to reach no more than two orders of magnitude¹⁰. The combined action of electromagnetic and chemical enhancement mechanisms is referred to as surface-enhanced resonant Raman scattering with multiplied enhancement coefficients.

Although both mechanisms combine their enhancements to reach better signal gains, probing them separately is crucial for understanding their physics. Electromagnetic enhancement is universal for all types of molecules and can be controlled and optimized by specially designed SERS-active nanostructures.

For applications of SERS in ultrasensitive detection, not only the values of the enhancement factor, but the range of action as well are key aspects. In the literature there is still some ambiguity concerning the last aspect of EM enhancement mechanism, what in a certain extent restricts the applications of SERS in analytical methods.

In most previously published investigations of SERS distance dependence, the Raman-active adsorbate was spaced from the surface using self-assembled monolayers of long organic molecules chemisorbed to the metal surface and thus the overall effect was subject to interplay of chemical and EM enhancement mechanisms or even suffered from modification of the metal surface electron states. Several studies^{17,18} performed on long chains of alkanethiols attached to silver surfaces show that the enhancement for remote chemical groups vanishes at extremely short distances (2–3 nm), which is in accordance with the theoretically predicted power law¹⁷ $\sim (1 + \frac{h}{r})^{-10}$ derived for a chaotic array of *non-interacting* nanoparticles, where r is the mean radius and h is the molecule-to-surface distance. Experiments using spacers created on nanostructured surfaces by atomic

layer deposition of Al_2O_3 also show very short-range SERS enhancements¹⁹, possibly resulting from the modification of the metal surface properties during the atomic layer deposition process. Thus, in the above-mentioned cases it is unclear what type of SERS enhancement is probed – chemical, electromagnetic, or a combination of the two.

We present a study of SERS distance dependence that utilizes chemically passive, uniform spacer layers with controlled thickness. To this end, a silver-based, SERS-active surface is covered by a transparent dielectric layer of variable thickness, and analyte molecules are settled on top of the spacer. This approach enables a distinctive study of the pure EM properties of SERS enhancement, irrespective of the chemical enhancement aspects.

Experimental

The experimental samples were prepared using thermal vacuum deposition. Polished silicon plates were used as wafers for deposition of layered metal-dielectric structures. The sequence of layers was as follows: (a) a relatively thick (50 nm) silver screening layer; (b) an insulating silicon monoxide (SiO) layer with a thickness of 15 nm; (c) a SERS-active nanoparticle layer formed by a silver island film with mass thickness of 6 nm; and (d) a SiO dielectric spacer layer with variable mass thickness, ranging from 0 to 60 nm. The final passivating layer was intended to separate the analyte molecules from the metal nanoparticles, and it was the primary parameter of the examination. The morphology of the first three layers in the SERS substrates and the deposition parameters (rate, pressure, and temperature) were fixed throughout the experiments. The heating power was kept constant to provide deposition rates of 0.5 \AA/s for Ag, and 1.5 \AA/s for SiO. The deposition pressure was lower than 5×10^{-6} torr. The distance dependence of SERS enhancement was studied by varying the thickness of the passivating dielectric layer in different samples. The set of samples consisted of SERS substrates with passivating layer thicknesses varying from 0 to 60 nm, with increments of 10 nm. Additionally, the dependence was studied on the samples with continuously varying thickness of the passivating layer across the surface. These gradient samples benefit from guaranteed homogeneity of the SERS-active layers across the sample surface, with only one parameter being varied – the thickness of SiO spacer. To produce such gradient substrates during the single-load of a vacuum deposition camera, a specially shaped mask was utilized (See bottom inset of Fig.1). The basic layers (a),(b), and (c) were deposited while the opening in the mask was precisely against the substrate surface, allowing the particle beams to settle homogeneously onto the surface. After the SERS-active layer was deposited, the axial-symmetric mask was set to rotation with rate 15 r/min, and the time-averaged exposure for the passivating layer became a variable function of the radial coordinate in accordance with the mask profile.

The surface morphology of the samples was studied using an electron beam microscope (EBM) Jeol model JSM

7001F with a resolution of 1 nm. The gradient profile of the passivating layer across the substrate was defined by EBM analysis of the sample cross section. The gradient SiO layer was sandwiched between two 50-nm-thick silver layers, and the cross section of this structure was analyzed and evaluated by the EBM. The thickness calibration curve of the gradient profile was plotted in coordinates (radial displacement–thickness). Independently, the thickness calibration was evaluated numerically based on the shape of the mask, and both calibration curves are plotted in Fig.1. Furthermore, EBM measurements were important for ascertaining that the SiO spacer layer is pinhole free and that it does not affect the characteristics of measured distance dependence. For this purpose, an additional 50-nm-thick layer of Ag was deposited on top of the passivating SiO layer to obtain an EBM-image with better contrast (See bottom-left inset of Fig.1). By analyzing EBM images taken at different spacer thicknesses, we determined that the spacer layer is pinhole free at spacer thicknesses greater than 15 nm.

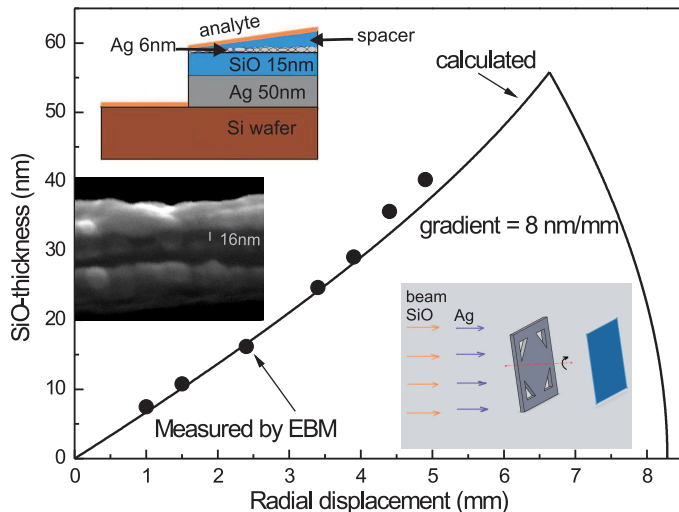


FIG. 1: The calibration curve of a gradient profile used for deposition of a passivating SiO layer. The smooth curve represents the result of a numerical evaluation based on the mask shape. The symbols are extracted from EBM imaging of the cross section of layered structure. The top inset illustrates the morphology of the SERS substrate with a metal island film covered by a dielectric layer with gradually increasing thickness. The bottom-right inset is an illustration of the vacuum deposition process with a rotating mask. The bottom-left inset shows the EBM image of cross section of the substrate covered by the 16 nm SiO layer and 50 nm Ag layer.

Different types of analytes were used to probe SERS enhancement: Rhodamine 6G (R6G) and β -carotene dyes, and colorless adenosine. Rhodamine 6G and β -carotene were deposited on substrates by spin-coating $10 \mu\text{L}$ drops of $1 - \mu\text{M}$ and $10 - \mu\text{M}$ ethanol solutions at 4000 r/min until drying was complete. Adenosine was dried out from a $2 \mu\text{L}$ drop of $200 \mu\text{M}$ water solution. These representatives were chosen because of their

qualitatively different properties as Raman-active agents: both dye molecules have strong Raman activity, but differ in fluorescence activity – Rhodamine 6G is fluorescent under 532 nm excitation as opposed to β -carotene at the same excitation. Colorless adenosine exhibits moderate Raman activity and is non-fluorescent. The distance dependence of SERS-enhancement on different types of molecules was tested in order to achieve a general view on whether resonant Raman enhancement plays a role in this effect.

Raman scattering experiments were performed at room temperature using the EnSpectr micro-Raman spectrometer with $\lambda_{exc} = 532$ nm excitation. The laser ($P = 10$ to $200 \mu W$) was focused onto the sample by a 20X microscope objective. The laser spot, sized $5 \mu m$, determined the spatial resolution of the surface-scanning method. The scanning was performed using the motorized XYZ-microstage Märzhäuser with a resolution of $0.1 \mu m$. The exposure time for each spectrum was set as 1 s.

Results and Discussion

Typical SERS spectra of analyte molecules are shown in Figs.2 and 3. The data shown in Fig.2 for β -carotene and adenosine are obtained for the series of substrates with nominally fixed morphology of the SERS-active nanostructure and with different thicknesses of the SiO spacer layer. The enhancement coefficient of nonpassivated SERS substrates was estimated to be between $\sim 5 \times 10^5$ and 10^6 , typical for such silver nanostructures. The homogeneity of each substrate was investigated via x - y scanning of the signal. On length scales of 2×2 mm, the rms deviation of the signal was found to be less than 3%, including deviations in the enhancement coefficient and in the surface distribution of the deposited molecules. A waterfall spectra (Fig.2A) explicitly displays the change in signal with increasing molecule-to-nanoparticle layer separation. The inset shows the dependence of the intensity of the strongest line with a Raman shift of 1525 cm^{-1} on the spacer thickness. The dependence is rather weak below the 30 nm separation, after which an abrupt collapse of signal is observed. Similar behavior is observed in the series of substrates with another analyte molecule – adenosine– applied using the $200 - \mu M$ water solution (Fig.2B). Here, the intensity of the 735 cm^{-1} line was analyzed. Despite the common trend of the distance dependencies that is obvious from these data, some inconveniences are unavoidable in this scheme of experiments. They include fluctuations in the output parameters of the substrates for each process of vacuum deposition, fluctuations in the analyte molecule deposition conditions, and the few points in this dependence.

Therefore, we prepared and analyzed another type of sample, having SERS substrates with the spacer layer thickness increasing in a smooth gradient. Considering the characteristic length scale of the distance dependence, the parameters for vacuum deposition of the SiO spacer layer were chosen such that spacer thickness gradually increased from 0 to ~ 50 nm, with a surface span of

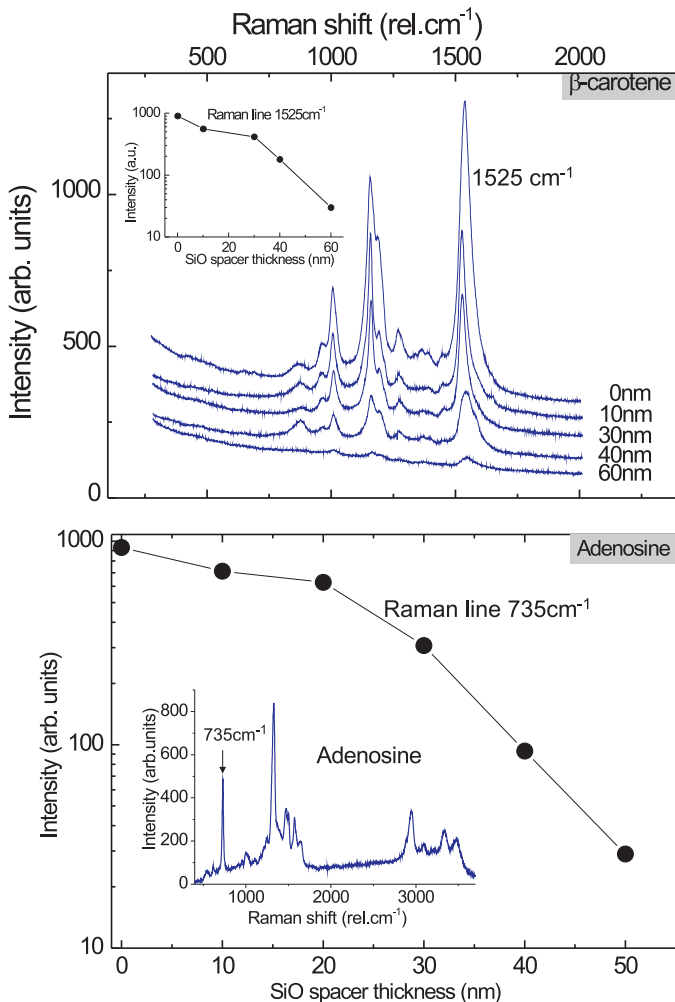


FIG. 2: (A) SERS-spectra of β -carotene molecules applied over the SiO spacer layer with thickness from 0 to 60 nm. The inset shows the plot of the 1525 cm^{-1} Raman line intensity as a function of spacer thickness. The molecules were deposited via spin-coating of $10 \mu L$ drop of $10 \mu M$ ethanol solution. Excitation power is $200 \mu W$ at 532 nm and exposure time is 1 s. (B) Plot of the SERS signal distance dependence for the 735 cm^{-1} Raman line of adenosine molecules, deposited from the $2 \mu L$ drop of $200 - \mu M$ water solution. Discrete points correspond to the signal obtained for substrates with SiO spacer thickness varying from 0 to 50 nm. The inset shows a typical SERS spectrum of adenosine.

8 mm. The gradient samples were spin-coated using solutions of Rhodamine 6G and β -carotene molecules. The spectra were recorded and analyzed across the gradient sector of the sample surface such that the integral intensities of several Raman lines were calculated and plotted as an image plot shown in the inset of Fig.3A. The image plot represents the distribution of the SERS signal from β -carotene on the gradient sector of the SERS substrate. The distance dependence of the 1525 cm^{-1} Raman line intensity was extracted from this 2D-array

of data points along the bisecting line. The resulting smooth dependence is shown in Fig.3A. It exhibits shelf-like behavior from 0 to ~ 25 nm and decreases rapidly at distances greater than 30 nm. Similar dependence was observed for R6G molecules, as shown in Fig.3B.

Note that the absolute values of SERS signal per molecule and per unit power of optical excitation differ by orders of magnitude for the different molecules used. For colorless adenosine molecules, the SERS spectrum is the weakest, whereas for the R6G dye molecules with absorption maximum at 523 nm the SERS is resonant and the resulting cross section is stronger by nearly three orders of magnitude. Irrespective of these dramatic differences in SERS cross sections, all three types of analyte molecules manifest similar distance-dependence behavior with a critical length parameter of approximately 25-30 nm.

In essence the experiment proves that the applied method directly probes the EM mechanism of SERS enhancement and excludes aspects such as chemical enhancement of the "first layer" of molecules or any other resonant contributions to the signal. The distance range of SERS enhancement should depend on the morphology of SERS-active layers and reflect the surface plasmon localization properties.

A length scale of 30 nm substantially exceeds the mean radius of nanoislands, and thus, the measured distance-dependence is in marked contrast with the well-known power law $\sim (1 + \frac{z}{r})^{-10}$ theoretically predicted for the chaotic array of independent nanoparticles. However, the observed shelf-like dependence indicates the existence of a new lengthscale in metal nanoparticle ensembles. Since this length scale manifests in the EM enhancement range, and the EM enhancement is in turn caused by the field distribution of surface plasmon polaritons (SPP), one may conclude that, firstly, SERS enhancement is determined by the *collective* surface plasmon polaritons in ensembles of neighboring nanoislands, and secondly, the work range of SERS enhancement should be determined by the penetration depth of the SPP electric field to the dielectric media.

In order to estimate this attenuation length SERS-active layers of silver islands can be roughly modeled as a thin, flat metallic layer sandwiched between two dielectric slabs. According to classical electrodynamics, the penetration depth of the SPP electric field in the dielectric is

$$\ell_p \sim \frac{\lambda_0}{2\pi} \frac{\sqrt{|\varepsilon_m(\omega) + \varepsilon_d|}}{\varepsilon_d},$$

where λ_0 is the vacuum wavelength of exciting EM-field, $\varepsilon_m(\omega)$ is the dielectric function of the metal, and ε_d is the average dielectric constant of the surrounding dielectric. In the case of silver islands surrounded by the 15 nm SiO layer and air and wavelength $\lambda_0 \sim 530$ nm we substitute $\varepsilon_d \approx 4$, and from Ref.20, we use $\varepsilon_m \approx -12 + 0.3i$ to obtain $\ell_p \approx 60$ nm. Using these substitutions, we find that the length parameter for the EM-field intensity, probed in

optical experiments, is half as long – $\ell_I \approx \ell_p/2 \approx 30$ nm – which is in reasonable agreement with measured values.

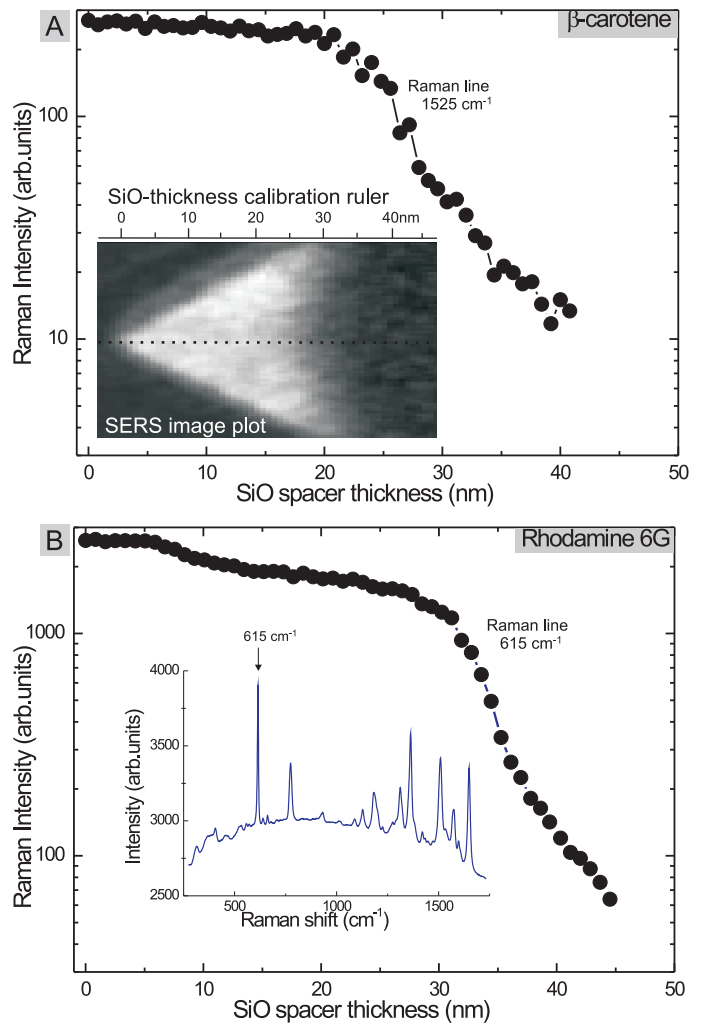


FIG. 3: SERS signal distance dependencies obtained for substrates with gradually increasing SiO spacer thicknesses across the surface. (A) Data for 1525 cm^{-1} Raman line of β -carotene. The inset shows the image-plot of the Raman line intensity over the substrate surface. The brightness of points represents the level of Raman signal, and the triangle sector corresponds to the SERS-active area of the sample with Raman signal diminishing from the vertex to the base. The main plot is extracted from data points along the triangle bisecting dotted line. The upper ruler on the image displays the scale of spacer thickness across the bisecting line. (B) Analogous continuous distance dependence plot measured for Rhodamine-6G molecules with SERS spectrum is shown in the inset. Excitation power is 10 μW at 532 nm and exposure time is 1 s.

Conclusion

In conclusion, this work studied the distance dependence of SERS enhancement of silver nano-island films. The layered Ag/SiO SERS substrates with fixed morphology were coated with an optically transparent passivating spacer layer composed of SiO, with variable thick-

ness, and the signal dependence on the thickness of the spacer layer was studied. Different types of analyte molecules showed qualitatively coinciding results. The SERS enhancement reduced slightly (less than half) up to distances of ~ 30 nm, after which it reduced abruptly. These results indicate that for such SERS substrates, enhancement coefficients on the order of 10^6 are primarily earned by long-range near-field effects and are independent of the effects from hot-spots localized in the narrow gaps between adjacent particles. Although the exact origin of the characteristic length scale of 30 nm is not clear now, the fact that it far exceeds the mean radius of silver nanoislands implies that the nature of field enhancement resides in the collective plasma response of *particle arrays* and not in individual particles. The length scale is presumably related to the spatial spread (or depth of penetration to the dielectric) of collective surface plasmon polaritons. To clarify this, additional research that inspects the SERS enhancement of nanoparticle agglomerations of different sizes is needed.

By employing the weak distance dependence of SERS-enhancement of 2D nanoparticle arrays up to distances 30 nm, a new type of SERS-substrates might be devel-

oped with the passivating layer of chemically passive and optically transparent dielectric deposited on top of metal nanostructures of any quasi-2D morphology. Virtually all key enhancement properties of a SERS substrate should be preserved, yielding a surface that is cleanable, non-expendable, and free of air degradation. This method of conservation may help extend the life of most effective and quite expensive (e.g., nanolithographically produced) SERS substrates, thus making them more profitable.

Another application of long-range SERS enhancement lies in the study of optical phenomena in low dimensional carrier systems based on solid-state structures. This method is applicable even if low dimensional objects are located at some depth-distance away from the surface.

Acknowledgments

The authors acknowledge support from the Russian Foundation for Basic Research.

-
- ¹ M. Fleischmann, P. J. Hendra and A. J. McQuillan, Chem.Phys.Lett. **26**(2), 163-166 (1974).
² D. L. Jeanmaire and R. P. Van Duyne, J. Electroanal. Chem., **84**, 1-20 (1977).
³ M. G. Albrecht and J. A. Creighton, Journal of the American Chemical Society, **99**(15), 5215 (1977).
⁴ K. Kneipp, D. Fessler, Chem. Phys. Lett., **106**, 498 (1984).
⁵ K. Kneipp, Y. Wang, H. Kneipp, et al., Phys.Rev.Lett. **78**, 1667 (1997).
⁶ J. I. Gersten, A. Nitzan, J. Chem. Phys. **75**, 1139 (1981).
⁷ S. L. McCall, P. M. Platzman, P. A. Wolff, Phys. Lett. A **77**, 381 (1980).
⁸ D. -S. Wang, M. Kerker, H. W. Chew, Appl. Opt. **19**, 2315 (1980).
⁹ M. Moskovits, Rev. Mod. Phys. **57**, 783-826 (1985).
¹⁰ A. Otto, In Light scattering in solids IV. Electronic scattering, spin effects, SERS and morphic effects; M. Cardona, G. Guntherodt, Eds.; Springer-Verlag: Berlin, Germany, 1984.
¹¹ A. Otto, I. Mrozek, H. Grabhorn, W. J. Akemann, J. Phys. Condens. Matter **4**, 1143 (1992).
¹² M. Kerker, O. Siiman, L. A. Bumm, D. -S. Wang, Appl. Opt. **19**, 3253 (1980).
¹³ D. -S. Wang, M. Kerker, Phys. Rev. B **24**, 1777 (1981).
¹⁴ V. M. Shalaev, Phys. Rep. **272**, 61 (1996).
¹⁵ V. M. Shalaev, A. K. Sarychev, Phys. Rev. B **57**, 13265 (1998).
¹⁶ V. A. Markel, V. M. Shalaev, P. Zhang, W. Huynh, L. Tay, T. L. Haslett, M. Moskovits, Phys. Rev. B **59**, 10903 (1999).
¹⁷ B. J. Kennedy, S. Spaeth, M. Dickey, and K. T. Carron, J. Phys. Chem. B **103**, 3640 (1999).
¹⁸ G. Compagnini, C. Galati, and S. Pignataro, Phys. Chem. Chem. Phys., **1**, 2351 (1999).
¹⁹ J. A. Dieringer, A. D. McFarland, N. C. Shah, et al., Faraday Discuss., **132**, 9 (2006).
²⁰ P. B. Johnson and R. W. Christy, Phys. Rev. B, **6**, 4370 (1972).